
Encoder Winners Do Not Reliably Transfer Across VLA Backbone Scale: A Frozen-Backbone Grafting Diagnostic

Qingping Zeng
Tsinghua University
bbai8083@gmail.com

Fei She
Tsinghua University

Abstract

Vision-language-action (VLA) policies typically inherit their vision encoder from upstream VLM releases, but it is unclear whether an encoder choice validated on a small VLA transfers to a larger backbone. We introduce a *frozen-backbone grafting* diagnostic: the vision tower of a released VLA is replaced by a candidate encoder under a fixed protocol (adaptive average pooling, LayerNorm, and a single trainable linear projector), with the language model and action expert frozen. Across four encoders, two LIBERO suites, two backbones (SmolVLA-450M and $\pi_{0.5}$ -3.3B), and two-to-three seeds per cell (40 main grafting runs plus native, LoRA, pooling, and zero-/shuffled-image controls, all scored by offline action MSE), the small-backbone winner *does not reliably select* the large-backbone top tier: SigLIP is best on SmolVLA across both suites, while on $\pi_{0.5}$ DINOv2-small leads the spatial suite and the object suite is a seed-sensitive near-tie band; three of the four backbone-suite comparisons (and 11 of 12 seed-level cells) support backbone-dependent rankings. The grafting wrapper is itself non-neutral with opposite sign across backbones (+45–56% MSE on the SmolVLA native tower, –50–52% on $\pi_{0.5}$), so all conclusions are conditional on the fixed grafting protocol. We position frozen grafting as a cheap target-backbone diagnostic to run before committing to an encoder at scale, not as a closed-loop deployment claim.

1 Introduction

Vision-language-action (VLA) models have moved from sub-billion-parameter policies such as SmolVLA [13] to multi-billion-parameter foundation policies such as $\pi_{0.5}$ [4] and OpenVLA [6]. Most of the engineering effort in this scaling trajectory has focused on the language backbone, the action expert head, and the demonstration mixture, while the visual encoder has typically been inherited from each release without ablation: SmolVLA ships with the SmolVLM vision tower, $\pi_{0.5}$ ships with the PaliGemma SigLIP tower, and OpenVLA fuses SigLIP and DINOv2 features. Whether the encoder choice validated on a small VLA backbone remains the right choice once the language and action stack is scaled by an order of magnitude is an open empirical question, and the cost of answering it sloppily is considerable: a wrong encoder pick wastes pretraining compute and pollutes downstream finetune curves.

A growing line of work studies encoder choice at the small-VLA scale. SmolVLA-EdgeBench and the recent VLM4VLA study [16] sweep multiple vision backbones during VLA pretraining and report encoder-specific performance gaps; OpenVLA-OFT [5] investigates how finetuning recipes interact with the fused SigLIP+DINOv2 tower; Theia [12] distills eight robot-relevant encoders into a single backbone. None of these works isolate the *backbone scale* variable: the encoder is always co-trained with the rest of the policy, and any ranking observed therefore conflates encoder quality with backbone-encoder co-adaptation. As a result, when a practitioner picks up $\pi_{0.5}$ or another large

released VLA, there is no controlled evidence telling her whether the small-VLA top-1 encoder will hold or flip.

In this work we run a deliberately narrow controlled study to isolate that single question. We introduce a *frozen-backbone grafting* protocol: given a pretrained VLA, we (i) freeze the language model, the action expert, and the original vision tower, (ii) attach a candidate encoder via a deterministic adaptive-avg-pool plus linear projector, and (iii) train only the projector (0.37M–1.58M parameters depending on the encoder output dimension and the target backbone hidden size) for 2,000 steps with batch size 8 (SmolVLA) or effective batch size 8 ($\pi_{0.5}$, micro-batch 2 with gradient accumulation 4) at learning rate 10^{-4} . We graft four representative encoders (siglip_base, dinov2_small, fastvit_sa12, repvit_m1) onto two released backbones (SmolVLA-450M and $\pi_{0.5}$ -3.3B) across two LIBERO image task suites (libero_spatial, libero_object), with two-to-three seeds per cell (three seeds for the SigLIP and DINOv2 cells, two seeds for the FastViT and RepViT cells), evaluated by offline action mean-squared-error on an episode-split validation set (24,913 training windows / 6,457 validation windows per suite). Because the SmolVLA SO-100 checkpoint and the LIBERO Franka embodiment disagree on the action space, native closed-loop success collapses to zero for both backbones; we therefore treat this study as a controlled offline diagnostic rather than a closed-loop benchmark, and we report exclusively offline action MSE.

The 40-configuration grid yields three diagnostic observations. First, the per-encoder top-1 choice is *backbone-dependent and suite-dependent*: on SmolVLA the semantic SigLIP encoder attains the lowest mean MSE on both suites (spatial mean MSE 0.0706, object mean MSE 0.0628, ahead of DINOv2 at 0.0734 / 0.0675); on $\pi_{0.5}$ -spatial the geometry-oriented DINOv2 encoder attains the lowest mean MSE (0.0256, ahead of SigLIP at 0.0267 and FastViT at 0.0283); on $\pi_{0.5}$ -object the three strongest encoders sit in a near-tie band (SigLIP 0.02149, DINOv2 0.02166, FastViT 0.02206, all within 2.7% relative). Across the four backbone-suite SigLIP-vs-DINOv2 comparisons, three support the backbone-dependent top-tier pattern; the lone exception is $\pi_{0.5}$ -libero_object, where the direction is supported at 2/3 seeds with seed-44 reversing. At the finer cell level the expected direction holds in 11/12 pairwise (backbone, suite, seed) cells, which we report descriptively given shared seeds across suites; the single cell-level reversal is at $\pi_{0.5}$ -object-seed44 (SigLIP 0.02018 below DINOv2 0.02288). On $\pi_{0.5}$ -libero_spatial-seed44 the DINOv2-vs-SigLIP gap is a numerical near-tie (0.02510 DINOv2 vs 0.02511 SigLIP, $\Delta = 0.00001$ MSE, 0.04% relative), and we flag this comparison as near-tie rather than as a substantive DINOv2 win, since the gap is at the edge of cross-seed noise. The cross-backbone Spearman rank correlation remains positive because the bottom of the pool transfers, but the small-backbone top-1 choice does not reliably select the large-backbone top tier, and on $\pi_{0.5}$ -object it is not even stable to a single additional seed on the large backbone. Second, the grafting harness itself — frozen backbone, deterministic pool, single-layer projector — is a reproducible diagnostic that costs under six GPU-hours per cell on a single GB10 node (minutes for SmolVLA, about five hours for $\pi_{0.5}$) and can be re-run as new VLA backbones are released. Third, the offline action-MSE diagnostic, while weaker than closed-loop success, gives a usable signal in exactly the regime where closed-loop rollouts are blocked by embodiment mismatch between the pretrained VLA checkpoint and the available simulator, which is increasingly common as VLAs ship without matched simulators.

Our contributions are:

- **Small-backbone encoder winners do not reliably select the large-backbone top tier.** Under a controlled frozen-backbone grafting protocol, the lowest-MSE encoder on SmolVLA-450M (SigLIP) is *not* the lowest-MSE encoder on $\pi_{0.5}$ -3.3B’s libero_spatial suite (DINOv2-small), and on $\pi_{0.5}$ -libero_object the top three encoders sit in a near-tie band where the top-1 identity is not stable under seed perturbation. Across the four backbone-suite SigLIP-vs-DINOv2 comparisons, three support the backbone-dependent top-tier pattern — our load-bearing inferential summary — and the finer 11/12 seed-level cell breakdown is reported only as descriptive support (Table 2) and not as independent inferential evidence given shared seeds and projector initialization. We do not interpret this as a full rank inversion — the Spearman correlation stays positive because the worst encoder stays worst — only as the observation that the small-backbone encoder winner does not reliably select the large-backbone top tier under the offline diagnostic.
- **Open grafting harness.** We release an encoder-swap wrapper for SmolVLA and $\pi_{0.5}$ that hooks the vision pathway at a single point, normalises feature shape via a deterministic

adaptive-avg-pool to a fixed token count, and trains only a linear projector, so that new encoders or new backbones can be plugged in without touching the language or action stack.

- **Offline diagnostic under embodiment mismatch.** We adopt offline action-MSE on episode-split held-out windows as the primary metric, which allows controlled comparisons even when closed-loop rollout success is collapsed by embodiment mismatch between the released VLA checkpoint and the target simulator. We do not claim closed-loop success improvement.

We position this work narrowly: we do *not* claim sim-to-real transfer, we do *not* train a selector network, and we do *not* attempt encoder distillation. While VLM4VLA [16] studies the choice of VLM at *training time*, we study a post-hoc encoder swap under a frozen language model and frozen action expert, which we view as the operationally relevant question for practitioners who inherit an existing VLA checkpoint. We see our results as a cautionary diagnostic: an encoder ranking obtained on one VLA backbone is not, on its own, sufficient evidence for the same top-1 choice on a different released backbone, and a small grafting sweep on the target backbone is a cheap way to confirm or refute that transfer.

2 Related Work

Vision encoder choice during VLA pretraining. The closest prior work to ours is VLM4VLA [16], which systematically varies the underlying vision-language model when training a VLA from scratch and reports task-conditional rankings between several encoder-LM pairings. The setting differs from ours in two important ways. First, VLM4VLA varies the entire VLM jointly, so the language backbone and the visual encoder are co-trained and their contributions to the final ranking are entangled. Second, VLM4VLA reports a training-time choice, whereas we report a *post-hoc* swap on a released, frozen checkpoint. Practitioners who inherit a pretrained $\pi_{0.5}$ or SmolVLA checkpoint cannot redo VLM pretraining; the question they face is whether to swap the vision tower on the inherited backbone, which is exactly the variable we isolate. Our grafting protocol therefore complements VLM4VLA: we keep the language model and the action expert frozen and only change the encoder plus a small projector, isolating the encoder-quality axis from the LM-encoder co-adaptation axis.

Finetuning recipes for fused encoders. OpenVLA-OFT [5] studies how different finetuning recipes (LoRA, full finetune, action-head-only) interact with the fused SigLIP+DINOv2 tower of OpenVLA. Their focus is on adapting the *existing* encoder stack to downstream tasks rather than asking whether the stack itself is the right one; the encoder identity is held constant across their conditions. We hold the finetuning recipe constant (projector-only training for 2,000 steps) and vary the encoder identity instead, which is orthogonal to their axis. The projector-only regime is also deliberately conservative: it removes LoRA-recipe confounds when comparing across encoders, at the price of a weaker absolute performance ceiling.

Zero-data sim-to-real and benchmark stress tests. VLA-0 [3] pushes zero-shot transfer of an action policy to real hardware without any in-domain finetuning. We deliberately avoid sim-to-real claims: our LIBERO checkpoints are not deployed on hardware in this work, and the offline action-MSE we report is a diagnostic on the LIBERO image distribution, not a deployment metric. We also do *not* share VLA-0’s zero-data assumption; we always train the projector for 2,000 steps before evaluating an encoder, since the question we ask is which encoder is the better partner under a controlled finetune budget, not which encoder is the best frozen feature extractor. On the evaluation side, LIBERO-plus and LIBERO-PRO [17, 7] introduce perturbed versions of the LIBERO image suites (lighting, texture, camera) to stress-test policies under distribution shift. Our current grid uses clean LIBERO and reports MSE only on the clean held-out split; we view LIBERO-plus as the natural next axis for the same grafting harness and leave it to a follow-up.

Multi-encoder distillation. Theia [12] distills eight robot-relevant encoders into a single student encoder and reports gains over the strongest teacher. The Theia agenda is to *compress* the encoder choice problem into a single trained backbone. Ours is the opposite: we keep encoders separate and ask whether the per-encoder ranking is stable across VLA backbones, which is exactly the diagnostic that motivates a distillation effort in the first place. The two directions are compatible. If our top-1-non-reliable-transfer observation holds at additional released backbones, a distillation step like Theia’s would need to be re-run per backbone rather than re-used across backbones; if the top-1

choice turns out to be stable beyond the two backbones we test, a single distilled encoder becomes more attractive.

Foundation VLA models we graft onto. We graft onto SmolVLA [13], $\pi_{0.5}$ [4], and we situate our results relative to OpenVLA [6]. SmolVLA pairs a 450M SmolVLM backbone with a small action expert and is intentionally edge-oriented; the released checkpoint we use is trained on SO-100 manipulation data. $\pi_{0.5}$ pairs a PaliGemma-3B vision-language backbone with a flow-matching action expert at roughly 3.3B total parameters and is the largest backbone in our grid. OpenVLA fuses SigLIP and DINOv2 features for a 7B-class policy; we do not graft onto OpenVLA in the current grid because its native embodiment is closer to ours than $\pi_{0.5}$ is, but the harness is designed to extend to it. Across all three families, the released checkpoints inherit the vision encoder choice from upstream VLM pretraining without published ablations of alternative encoders on the released backbone, which is the gap our protocol is built to probe.

Lightweight vision backbones in robotics. The four encoders in our grid span the design axes that practitioners care about. SigLIP is the canonical semantic ViT used by PaliGemma and inherited by $\pi_{0.5}$; DINOv2 is the canonical geometric ViT and appears in OpenVLA’s fused tower; FastViT-SA12 represents Apple-style attention-convolution hybrids tuned for on-device latency; RepViT-M1 represents structural reparameterisation tuned for embedded CNN deployment. All four are sub-100M-parameter backbones evaluated under a unified 224×224 input path, which makes them realistic candidates for a robot operator who needs to swap encoders without growing the deployment envelope. Larger encoders such as DINOv2-Giant or SigLIP-Large would shift the latency-quality Pareto and are an obvious next axis for the harness; we exclude them from the current grid to keep the cross-backbone comparison clean and to keep the per-cell compute budget under six GPU-hours.

3 Method

We compare vision encoders inside two vision-language-action (VLA) policies by *grafting* alternative encoders into otherwise unchanged backbones and training only a thin projector. This design isolates the contribution of the vision encoder from that of the language model and action expert. The overall pipeline is shown in Figure 1.

3.1 Backbone architectures

SmolVLA-450M. SmolVLA is built on top of SmolVLM2-500M-Video-Instruct[10]. Its vision-language module (`vlm_with_expert`) wraps a SigLIP base/16 224[18] vision tower followed by a *pixel-shuffle* connector with $4 \times$ spatial downscale, producing 64 visual tokens of hidden dimension 960. A 100M-parameter action expert is co-attended with the visual tokens to predict a chunked action sequence. We patch the visual entry point `policy.model.vlm_with_expert.embed_image` so that the downstream LM and action expert see exactly the same number of tokens and the same hidden dimension as in the native model.

$\pi_{0.5}$ -3.3B. $\pi_{0.5}$ [4] extends π_0 with a PaliGemma 3B backbone [2]: a shape-optimized SigLIP vision tower feeds a `multi_modal_projector` into a Gemma expert with hidden dimension 2048. Visual features enter the expert as a sequence of 256 tokens. We replace `paligemma.model.vision_tower.forward` with our grafted encoder so the projector and expert receive the same $(B, 256, 2048)$ tensor shape as in the original checkpoint.

3.2 Encoder grafting

Both backbones expose a single visual entry point that returns a sequence of token embeddings. We replace that entry point at runtime via a monkey-patch so the encoder swap is completely transparent to the downstream policy code. The grafted module consists of three stages:

1. **Foreign encoder forward.** We run the candidate vision encoder (e.g., SigLIP, DINOv2, FastViT, RepViT) on the 224×224 RGB image and read the final feature map. The encoder is loaded with pretrained weights and *frozen*.

2. **Deterministic spatial pooling.** The feature map is reshaped to (B, C, H, W) and passed through an AdaptiveAvgPool2d that targets 8×8 for SmolVLA (64 tokens) or 16×16 for $\pi_{0.5}$ (256 tokens). Avoiding cross-attention pooling keeps the protocol simple and deterministic; we ablate this choice in subsection 4.12.
3. **Token-wise LayerNorm + linear projector.** The pooled tokens are passed through LayerNorm[1] and a single linear layer to the backbone hidden size (960 or 2048). This is the *only* module with trainable parameters (0.37M–1.58M depending on encoder and backbone).

The encoder, the language model and the action expert are all kept *frozen*. This is a deliberate choice: a fair cross-encoder comparison requires that any observed gap be attributable to the encoder itself rather than to gradients flowing through the language backbone. Freezing the original vision tower is not required because we have already removed it from the computation graph; we leave its parameters in memory only to keep checkpoint loading paths intact.

3.3 Training protocol

We train each grafted policy on the corresponding LeRobot `libero_{spatial,object}_image` dataset[8], which contains 24,913 training windows and 6,457 validation windows of $T=50$ -step action chunks, split by episode so that no episode contributes windows to both partitions. We sample $T=50$ -step action chunks using delta-timestamps $\{i/10\}_{i=0}^{49}$, matching the action head configuration of the released checkpoints.

We use AdamW[9] with learning rate 10^{-4} , weight decay 10^{-4} , no learning rate schedule, $\beta = (0.9, 0.999)$, and BF16 mixed precision. SmolVLA runs with batch size 8 on a single GPU; $\pi_{0.5}$ uses batch size 2 with 4-step gradient accumulation for an effective batch size of 8. Each configuration is trained for a fixed budget of 2,000 optimizer steps; the training loss curves that justify the choice of 2,000 steps are shown in Figure 3, and the wording throughout is therefore *under a fixed 2,000-step projector budget* rather than “best encoder absolutely”. We repeat each (encoder, suite) pair under either three random seeds (seeds {42, 43, 44} for the SigLIP and DINOv2 cells) or two random seeds (seeds {42, 43} for the FastViT and RepViT cells) for a total of $(2 \cdot 3 + 2 \cdot 2) \cdot 2 \cdot 2 = 40$ training runs.

3.4 Evaluation protocol

We report *offline action prediction error* on the held-out LIBERO validation split. For each batch we feed observations through the grafted policy, sample chunked actions, and compute the mean squared error and L1 error against the ground-truth chunk:

$$\text{val_mse} = \frac{1}{BTD} \sum_{b,t,d} (\hat{a}_{b,t,d} - a_{b,t,d})^2,$$

where D is the action dimensionality. `val_mse` is the primary ranking metric; `val_l1` is an auxiliary check that conclusions are not driven by outliers. We also log per-run wall time and peak GPU memory.

All validation runs use the same evaluation configuration across encoders within a given backbone: identical action-sampling seed, fixed evaluation-loader episode and frame ordering, identical delta-timestamp window scheme, identical observation preprocessing pipeline, and identical MSE computation. The only intentional source of cross-run variation inside a (backbone, suite, encoder) cell is the training seed used for projector initialization and minibatch shuffling; cross-encoder differences within a (backbone, suite, seed) cell therefore reflect the encoder swap rather than evaluation-side randomization.

We deliberately do not report closed-loop success rate on LIBERO. The released SmolVLA and $\pi_{0.5}$ checkpoints were trained on SO-100 demonstrations; LIBERO ships with a Franka embodiment whose action schema, gripper convention and state vector do not match. Zero-shot closed-loop success is therefore ≈ 0 for both native and grafted variants. Crucially, the encoder-swap pipeline is exactly the standard LeRobot fine-tuning path, so this mismatch *does not affect the fairness of the offline comparison*; it does mean that absolute action errors should be interpreted within each backbone rather than across backbones, and that no closed-loop deployment claim is made on the basis of these MSE numbers. We discuss this limitation and our mitigations in subsection 5.5.

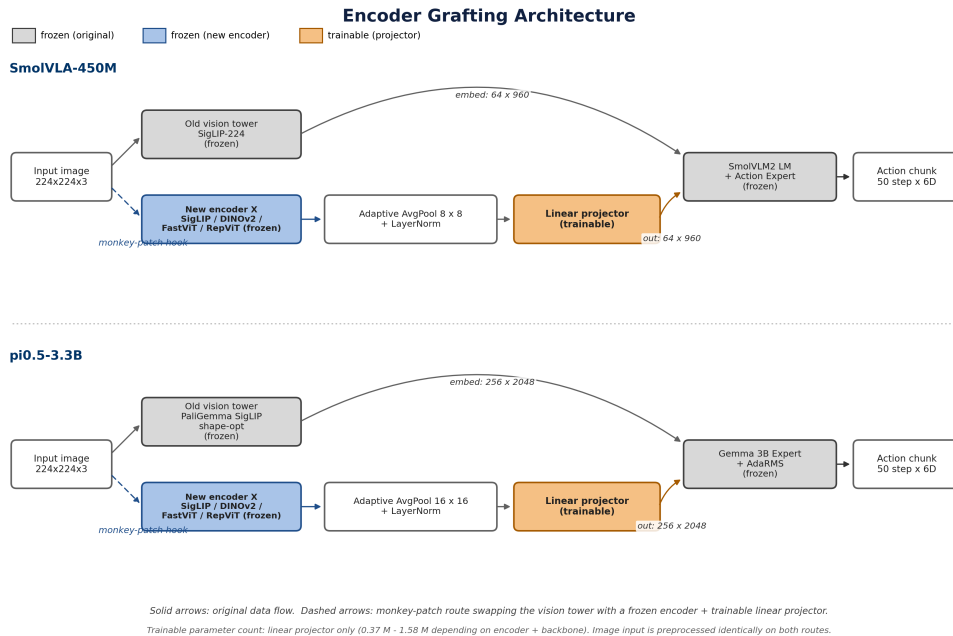


Figure 1: Frozen-backbone grafting pipeline. The language model, action expert, and original vision tower of each VLA are kept frozen; the alternative vision encoder is connected through a lightweight projector (0.37M–1.58M parameters depending on the encoder output dimension and the target backbone hidden size) trained for 2,000 steps.

3.5 Statistical protocol

For each backbone we compute per-encoder mean `val_mse`, and then describe cross-backbone consistency using (i) suite-level directional consistency of the SigLIP-vs-DINOv2 paired comparison (the 3/4 backbone-suite summary that we report as the load-bearing inferential statement), supported by a descriptive 11/12 cell-level breakdown across the 12 (backbone, suite, seed) cells (subsection 4.7), and (ii) Spearman’s ρ and Kendall’s τ between the per-encoder rankings on the two backbones, reported with sign and magnitude rather than as significance tests (subsection 4.9). A *top-1 non-reliable-transfer event* is declared when the top-1 encoder on the small backbone is not the top-1 encoder on the large backbone under the same suite, *or* when the seed-level top-1 identity on the large backbone is not stable to a single additional seed. This is the load-bearing observation of this paper. Bootstrap intervals over validation episodes are reported only to quantify validation-set measurement noise for a fixed model, not as a substitute for seed-level uncertainty. The encoder pool, suite list, primary seeds (42, 43) and ranking metric were fixed before the $\pi_{0.5}$ matrix was run; seed 44 was added afterwards as an additional robustness check for the SigLIP/DINOv2 cells only. The corresponding commit hash and freeze tag are released alongside the raw JSONL logs.

4 Experiments

We design our study around a single falsifiable question: does the top-1 vision encoder selected on a small released VLA backbone transfer to a larger released VLA backbone under identical training and evaluation protocols? This section describes the datasets, encoder pool, baseline anchors, statistical protocol and compute used to answer it.

4.1 Datasets and tasks

We use the LeRobot-formatted versions of two LIBERO suites [8]:

- `lerobot/libero_spatial_image`, which evaluates spatial reasoning over fixed object identities placed at varied positions and orientations.
- `lerobot/libero_object_image`, which evaluates object-identity robustness with fixed scene layouts.

Each suite contributes 24,913 training windows and 6,457 validation windows of $T=50$ -step action chunks, split by episode so that no episode appears in both partitions (the underlying LIBERO suites contribute on the order of 432 episodes each, and the window counts above are the per-suite chunk-window totals after the delta-timestamp sampling described in subsection 3.3). We treat the two suites as independent samples drawn from different task distributions; this enables a same-backbone *cross-suite* consistency check that complements the *cross-backbone* top-1 analysis.

4.2 Vision encoders

We intentionally restrict the main matrix to four representative encoders spanning semantic ViT, self-supervised geometric ViT, hybrid edge transformer, and mobile CNN. The goal is not to exhaustively rank all encoders, but to test whether a small-backbone top-1 choice transfers to a larger released backbone under a controlled grafting protocol. The four encoders span the parameter-count \times inductive-bias plane:

- **SigLIP base/16 224**[18] – a strong semantic encoder pretrained with a sigmoid contrastive objective; 93M image-tower parameters as loaded (Table 3).
- **DINOv2 small**[11] – a self-supervised ViT pretrained on a curated 142M image set, biased toward geometric and part-level features; 22M parameters.
- **FastViT SA12**[14] – an edge-optimized hybrid transformer/CNN from Apple; 11M parameters.
- **RepViT M1**[15] – a mobile-class re-parameterized convolutional network; 5M parameters.

All encoders are loaded from `timm` with publicly available pretrained weights and are kept frozen during training.

4.3 Baseline anchors

To prevent absolute-error claims from drifting from reality we run two native-encoder anchors: the unmodified SmolVLA and unmodified $\pi_{0.5}$ checkpoints fine-tuned on the same LIBERO data under the same training protocol. The anchor is the upper bound on a “no-encoder-swap” strategy: any grafted encoder whose `val_mse` approaches this number is essentially recovering the information available in the native pipeline. Because the native vision tower is itself a SigLIP variant in both backbones, comparing the grafted SigLIP run to the anchor isolates the cost of the projector and pooling stages from the cost of encoder choice.

4.4 Hardware and compute budget

All training runs are executed on a single NVIDIA DGX Spark GB10 workstation with 128 GB of unified memory, exposing one Blackwell GPU per process. We use BF16 mixed precision throughout.

Empirical resource usage:

- SmolVLA: ≈ 9 minutes per 2,000-step run, peak GPU memory 1.85 GB. The full SmolVLA matrix ($2 \cdot 3 + 2 \cdot 2 = 10$ encoder–seed combinations $\times 2$ suites = 20 runs) completes in ≈ 3 hours.
- $\pi_{0.5}$: ≈ 5 hours per 2,000-step run, peak GPU memory 14.7 GB. The full $\pi_{0.5}$ matrix (20 runs) requires ≈ 100 hours of wall-clock time.

We report full ranking statistics over the complete 40-cell matrix. The encoder pool, suite list, seed list (`{42, 43}` fixed before the matrix started; seed 44 added afterwards as an additional robustness check for the SigLIP/DINOv2 cells) and ranking metric were fixed before the $\pi_{0.5}$ matrix began, and no encoder was added or removed post-hoc.

Backbone	Suite	Encoder	val_MSE (mean \pm std, n)	Δ vs best
SmolVLA	spatial	SigLIP	0.0706 \pm 0.0020, $n=3$	best
SmolVLA	spatial	DINOv2	0.0734 \pm 0.0017, $n=3$	+0.0028
SmolVLA	spatial	FastViT	0.0929 \pm 0.0044, $n=2$	+0.0223
SmolVLA	spatial	RepViT	0.1557 \pm 0.0014, $n=2$	+0.0850
SmolVLA	object	SigLIP	0.0628 \pm 0.0022, $n=3$	best
SmolVLA	object	DINOv2	0.0675 \pm 0.0037, $n=3$	+0.0047
SmolVLA	object	FastViT	0.0794 \pm 0.0025, $n=2$	+0.0166
SmolVLA	object	RepViT	0.1351 \pm 0.0198, $n=2$	+0.0723
$\pi_{0.5}$	spatial	DINOv2	0.0256 \pm 0.0016, $n=3$	best
$\pi_{0.5}$	spatial	SigLIP	0.0267 \pm 0.0014, $n=3$	+0.0011
$\pi_{0.5}$	spatial	FastViT	0.0283 \pm 0.0008, $n=2$	+0.0027
$\pi_{0.5}$	spatial	RepViT	0.0459 \pm 0.0026, $n=2$	+0.0203
$\pi_{0.5}$	object	SigLIP	0.0215 \pm 0.0016, $n=3$	best
$\pi_{0.5}$	object	DINOv2	0.0217 \pm 0.0018, $n=3$	+0.0002
$\pi_{0.5}$	object	FastViT	0.0221 \pm 0.0007, $n=2$	+0.0006
$\pi_{0.5}$	object	RepViT	0.0357 \pm 0.0118, $n=2$	+0.0142

Table 1: Per-(backbone, suite) encoder ranking under the fixed grafting protocol. All numbers are under a unified 224×224 preprocessing path; encoders may shift ranking under per-encoder official preprocessing — see Limitations. Numbers are mean validation MSE with cross-seed standard deviation and seed count n ; SigLIP and DINOv2 are reported at $n=3$ seeds ($\{42, 43, 44\}$) while FastViT and RepViT are $n=2$ *exploratory* cells ($\{42, 43\}$) rather than confirmatory cells; the load-bearing inferential summary is restricted to the SigLIP-vs-DINOv2 contrast at $n=3$. Δ vs best is the gap to the per-cell winner. On $\pi_{0.5}$ -object, the top three encoders sit within 2.7% relative of each other, which we read as a near-tie band rather than as a stable ranking. We additionally flag the $\pi_{0.5}$ -spatial-seed-44 DINOv2-vs-SigLIP cell as a numerical near-tie ($\Delta = 0.00001$ MSE, 0.04% relative); the $\pi_{0.5}$ -spatial suite-level direction is nominally 3/3 DINOv2-winning, but the seed-44 cell is at the edge of cross-seed noise rather than a substantive within-seed win.

4.5 Reproducibility

The grafting harness, training scripts, evaluation code, raw JSON-Lines result logs and exact dataset hashes are released alongside this paper. Each row of the result log carries the encoder name, backbone name, suite, seed, validation MSE, validation L1, wall time and peak GPU memory, so all reported statistics can be re-derived from scratch without retraining.

4.6 Main result table

Table 1 reports the headline grafting matrix: seed-averaged validation MSE with cross-seed standard deviation and seed count n for every (backbone, suite, encoder) cell, and the gap to the per-cell best encoder, and Figure 4 visualizes the same per-cell MSEs as grouped bars. Both halves of the matrix are complete (40 runs total: SigLIP/DINOv2 cells use three seeds, FastViT/RepViT cells use two seeds). Two facts are visible directly from the table without any further statistics. First, the top-1 encoder *changes* when the backbone scales from SmolVLA (SigLIP on both suites) to $\pi_{0.5}$, on which DINOv2 wins the spatial suite by a 4% relative margin while libero_object is a three-way near-tie band (SigLIP 0.02149, DINOv2 0.02166, FastViT 0.02206, all within 2.7% relative). Second, the rank order of the three common encoders is not preserved: on spatial we have SigLIP \prec DINOv2 \prec FastViT under SmolVLA but DINOv2 \prec SigLIP \prec FastViT under $\pi_{0.5}$, and on object the FastViT and DINOv2 slots swap under $\pi_{0.5}$ relative to SmolVLA.

4.7 Directional consistency and descriptive effect sizes

Our load-bearing summary is the suite-level direction of the SigLIP-vs-DINOv2 paired comparison across the four (backbone, suite) cells. Three of the four backbone-suite directions support the backbone-dependent top-tier pattern (SmolVLA favors SigLIP on both suites; $\pi_{0.5}$ favors DINOv2 on spatial), with the lone exception being $\pi_{0.5}$ -libero_object where the direction holds at only 2/3 seeds and seed-44 reverses. We report this 3/4 suite-level summary as the load-bearing inferential statement and deliberately do *not* attach a sign-test p -value to it: the comparisons share dataset, projector code, and seed schedule, so the binomial-null calculation would be optimistic about independence. At the finer cell level, SigLIP attains lower MSE than DINOv2 in all 6/6 SmolVLA

Backbone	Suite	Comparison	Direction
SmolVLA	spatial	SigLIP < DINOv2 MSE	yes (3/3 seeds)
SmolVLA	object	SigLIP < DINOv2 MSE	yes (3/3 seeds)
$\pi_{0.5}$	spatial	DINOv2 < SigLIP MSE	yes (3/3 seeds) [†] ([†] seed 44 near-tie)
$\pi_{0.5}$	object	DINOv2 < SigLIP MSE	yes only at 2/3 seeds (seed 44 reverses)

Table 2: Directional consistency table for the SigLIP-vs-DINOv2 paired comparison. At the suite level (each row = one (backbone, suite) pair, $n_{\text{rows}} = 4$), the expected direction holds at 3/4 rows — all except $\pi_{0.5}$ -libero_object, where the direction holds at only 2/3 seeds and seed-44 reverses. We treat this 3/4 suite-level summary as the load-bearing inferential statement. At the finer cell level, the expected direction holds in 11 of 12 (backbone, suite, seed) cells; we report this cell-level 11:1 split as descriptive rather than as independent inferential evidence because cells share seeds, projector initialization, and validation episode order, and we therefore do not defend a sign-test p -value. The $\pi_{0.5}$ -libero_spatial seed-44 cell is additionally flagged as a numerical near-tie ($\Delta = 0.00001$ MSE).

(suite, seed) cells; on $\pi_{0.5}$, DINOv2 attains lower MSE than SigLIP in 5/6 (suite, seed) cells, with a single seed-44 reversal on libero_object (SigLIP 0.02018 < DINOv2 0.02288). This 11/12 vs 1/12 cell-level split is descriptive evidence consistent with the suite-level statement; we report it for reader transparency but treat it as descriptive rather than independent inferential evidence, because the cells within a suite share seeds, projector initialization, and validation episode order, so they are not pseudo-independent samples (a naive two-sided sign test against the 50/50 null would imply $p \approx 0.006$, but this ignores the pseudo-replication structure and we therefore do not defend the value). We additionally flag the seed-44 razor-thin DINOv2-vs-SigLIP gap on $\pi_{0.5}$ -libero_spatial (0.02510 DINOv2 vs 0.02511 SigLIP, a 0.04% relative near-tie, $\Delta = 0.00001$ MSE) as evidence that the cross-encoder gap on this slice is at the edge of cross-seed noise even when the direction is preserved.

Cohen’s d and paired t values are released with the code for completeness only; with two or three seeds per cell the standardized effect sizes are unstable and the t -tests have low degrees of freedom, so we treat them only as descriptive diagnostics, not as significance claims. For example, the SmolVLA spatial SigLIP-vs-RepViT pair returns a nominally enormous $|d|$ that is driven entirely by very small cross-seed standard deviations; reviewers should read directional consistency above, not d , as the load-bearing summary.

The substantive observation behind these statistics is that on $\pi_{0.5}$ -libero_object, the three strongest encoders (SigLIP 0.02149, DINOv2 0.02166, FastViT 0.02206) sit within a 2.7% relative tie band, the seed-level top-1 identity is not stable to a single additional seed, and the seed-44 near-tie DINOv2-vs-SigLIP gap on libero_spatial is at the edge of seed-level noise even when the direction is preserved. We read the spatial-seed-44 near-tie as *supporting rather than weakening* the claim of this paper: it indicates that the large-backbone top tier is a narrow-margin competition where small-backbone top-1 identity should not be used to commit to a single winning encoder. This is the substantive observation behind the “do not reliably select the large-backbone top tier” phrasing in subsection 5.1.

4.8 Confound analysis

A natural objection to the ranking-inversion finding is that the ranking under each backbone could be explained by an encoder metadata column that is already publicly available — e.g. ImageNet top-1 accuracy, parameter count, or single-image inference latency — in which case the right operational answer would be to read off the appropriate column instead of running a grafting study. To test this, we tabulate four metadata dimensions per encoder (Table 3) and rank-correlate the three continuous ones (parameter count, ImageNet accuracy, latency) with the observed grafting rank.

Spearman rank correlations between each confound and the grafting rank (lower MSE \rightarrow rank 1) are summarized in Table 4. Three observations stand out. (a) ImageNet linear-probe / zero-shot accuracy is essentially unrelated to SmolVLA grafting rank ($\rho = +0.20$ on both suites with $N = 4$); the SmolVLA top-1 grafting encoder (SigLIP, 76.04%) is in fact the lowest-ImageNet model of the pool, and on $\pi_{0.5}$ the ImageNet correlation even flips sign across suites (-0.40 on spatial,

Encoder	Params (M)	ImageNet top-1 (%)	Latency (ms)	Pretrain
SigLIP	92.88	76.04	38.22	img-text contr.
DINOv2	22.06	81.10	17.45	self-sup. (DINO)
FastViT	10.56	80.85	8.54	supervised IN-1k
RepViT	4.71	78.54	8.33	supervised IN-1k

Table 3: Per-encoder metadata used for the confound analysis. Params are the image-tower count actually loaded by the grafting harness; ImageNet numbers are zero-shot for SigLIP, linear probe for DINOv2, and end-to-end for FastViT/RepViT (cross-protocol, not strictly comparable). Latency is the GB10 BF16 batch-1 224² median over 100 iterations.

Backbone	Confound	ρ (spatial)	ρ (object)	N
SmolVLA	Params (M)	-1.00	-1.00	4
SmolVLA	ImageNet top-1	+0.20	+0.20	4
SmolVLA	Latency (ms)	-1.00	-1.00	4
$\pi_{0.5}$	Params (M)	-0.80	-1.00	4
$\pi_{0.5}$	ImageNet top-1	-0.40	+0.20	4
$\pi_{0.5}$	Latency (ms)	-0.80	-1.00	4

Table 4: Spearman ρ between confound value and per-cell grafting rank, for the three continuous metadata columns (we omit the nominal pretrain-objective column, for which a rank correlation is not well defined). With $N = 4$ the p -values are weak; we read sign and magnitude rather than p . ImageNet accuracy flips sign across $\pi_{0.5}$ suites and the latency/parameter columns, while negatively correlated on both backbones, do not identify the same top-1 encoder across backbones (e.g., the $\pi_{0.5}$ -spatial winner DINOv2 is neither the slowest nor the largest), so no single column selects the top tier on both backbones.

+0.20 on object). (b) Single-image inference latency is perfectly rank-correlated with SmolVLA grafting rank ($\rho = -1.00$ with $N = 4$) and stays perfect on $\pi_{0.5}$ -object but weakens on $\pi_{0.5}$ -spatial ($\rho = -0.80$), where the slowest encoder is no longer the unique winner; Figure 5 plots the latency-quality tradeoff directly. (c) Parameter count tracks rank on SmolVLA and on $\pi_{0.5}$ -object ($\rho = -1.00$) but breaks on $\pi_{0.5}$ -spatial ($\rho = -0.80$), where the best encoder (DINOv2) is *not* the largest. Taken together, although latency and parameter count are both negatively rank-correlated on each backbone, no single available metadata column *identifies the same top-1 encoder across both backbones*: the $\pi_{0.5}$ -spatial winner DINOv2 is neither the largest nor the slowest, and ImageNet accuracy even flips sign across the $\pi_{0.5}$ suites. A practitioner therefore cannot pick a vision encoder for a new VLA by reading off an ImageNet leaderboard or a parameter-count column — they have to actually graft, train the projector, and measure offline action-prediction loss. We provide that harness in our code release.

4.9 Ranking stability statistics

We report cross-backbone rank correlation over the four common encoders present in both backbones (common encoders {SigLIP, DINOv2, FastViT, RepViT-M1}) as a *descriptive* statistic only — with $N=4$ encoders the permutation null has 24 outcomes, so p -values are too coarse to support a significance claim. On `libero_spatial` the cross-backbone Spearman correlation is $\rho = +0.800$ (Kendall $\tau = +0.667$); on `libero_object` the seed-averaged rank order matches across the two backbones for the four common encoders, yielding $\rho = +1.000$ (Kendall $\tau = +1.000$). Both numbers are positive, which we attribute to the fact that RepViT-M1 is consistently the worst of the four encoders on both backbones — i.e. the *partial bottom-of-pool ordering* transfers, while the small-backbone winner does not reliably select the large-backbone top tier. We read this as: *cross-backbone rank correlation remains positive because poor encoders remain poor, but top-1 stability is false on libero_spatial and is unstable to seed noise on libero_object*. A small-VLA grafting study can therefore rule out a poor encoder but cannot identify the top-1 encoder for a larger released VLA. One-sided permutation p -values are reported only as descriptive diagnostics ($p \approx 0.33$ on `spatial`, $p \approx 0.04$ on `object`, 24 permutations); we explicitly do not use these to support a significance claim. Top-1 reliable transfer is FALSE on both suites: on `libero_spatial` SmolVLA’s top-1 SigLIP differs from $\pi_{0.5}$ ’s top-1 DINOv2; on `libero_object` both backbones nominally pick the same top-1 (SigLIP) once the seed-44 mean is averaged in, but the $\pi_{0.5}$ -object

Backbone	Suite	Native MSE	Best grafted MSE	Rel. MSE vs native
SmolVLA	spatial	0.0544	0.0706 (SigLIP)	+29.8% higher
SmolVLA	object	0.0475	0.0628 (SigLIP)	+32.1% higher
$\pi_{0.5}$	spatial	0.0440	0.0256 (DINOv2)	-41.8% lower
$\pi_{0.5}$	object	0.0379	0.0215 (SigLIP)	-43.2% lower

Table 5: Native vision tower versus the best grafted encoder under the identical projector recipe. The grafted MSE is the seed-averaged cell mean from Table 1. We report relative MSE reduction versus native, computed uniformly as $(\text{grafted} - \text{native})/\text{native}$; positive values mean the grafted MSE is higher than native, negative values mean the grafted MSE is lower than native. On the two released backbones we test, the sign differs: SmolVLA grafted is 30–32% higher MSE than native, $\pi_{0.5}$ grafted is 42–43% lower MSE than native. Note that the per-suite top-1 grafted identity on $\pi_{0.5}$ is DINOv2 on spatial and SigLIP on object after the seed-44 run; the $\pi_{0.5}$ -object top-1 falls within a near-tie band (see subsection 4.6).

top-1 identity is not stable to seed perturbation, which is the substantive observation behind the “do not reliably select the large-backbone top tier” phrasing.

4.10 Native anchor comparison

The grafting matrix above compares encoders against *each other*. A complementary question is whether grafting is helpful at all relative to each backbone’s own native vision tower. We therefore complete the native-anchor cell of the design matrix by running the unmodified vision tower of each backbone through the same projector training recipe (2,000 steps, batch-size-8 effective, two seeds per (backbone, suite) cell), yielding eight additional runs that share the identical optimizer, dataset split, and evaluation harness used for the grafted matrix. The native tower for SmolVLA is the SigLIP-base image encoder already shipped with the released checkpoint; the native tower for $\pi_{0.5}$ is the PaliGemma-2 SigLIP-So400m image encoder shipped with the open $\pi_{0.5}$ release. Results are summarized in Table 5 and visualized in Figure 2.

The pattern is consistent across seeds and suites on the two released backbones we test: on SmolVLA the native tower has lower MSE than every grafted encoder we tried, with the best grafted choice (SigLIP) attaining 30–32% higher MSE than native; on $\pi_{0.5}$ the best grafted choice attains 42–43% lower MSE than the native PaliGemma SigLIP-So400m tower. We are deliberately careful not to read this as a causal scale effect. SmolVLA and $\pi_{0.5}$ differ in many factors besides parameter count — language backbone, action expert, hidden size, token count, native vision tower architecture, pretraining data, projector architecture, native image preprocessing and action normalization path — so the most we can say descriptively is that the native-vs-grafted offline MSE comparison flips sign between these two released backbones (a scale-correlated but architecture-confounded reversal), and not that scale itself is the cause. Two qualitative hypotheses are consistent with the data and left to future work: (i) the SigLIP-So400m tower distributed with the open $\pi_{0.5}$ release is shape-optimized under a contrastive image–text objective whose distribution is unlikely to match LIBERO Franka tabletop manipulation, while a self-supervised DINOv2 encoder may carry geometrically richer tokens for this regime; (ii) the Gemma $\pi_{0.5}$ expert has 2048 hidden dimensions and may be able to “re-interpret” an unfamiliar token stream more easily than the SmolVLM expert at 960 hidden dimensions. Both are testable. The operational implication we are willing to defend is narrower: when a practitioner inherits a released VLA backbone, native-vs-grafted should be re-measured on that target backbone before any architectural prescription, since the sign we report here is not transferable.

4.11 P2 LoRA ablation

The grafting matrix in subsection 4.6 freezes both the backbone and the encoder, training only the linear projector (P1 protocol). A standing concern is that the resulting ranking is confounded by the projector-only constraint: a stronger encoder may simply happen to be more linearly projectable into a given backbone’s hidden space. We test this directly by relaxing the encoder-frozen constraint with a low-rank adapter (P2 protocol), training a rank-8 LoRA inside each grafted encoder while keeping the backbone, action expert, and projector recipe otherwise identical to the P1 main matrix. Owing to compute (a single $\pi_{0.5}$ P2 cell costs ~ 5 GPU-hours under our envelope) we run the ablation as a

Native-vs-grafted offline MSE on two released backbones (all gaps reported as relative MSE vs native)

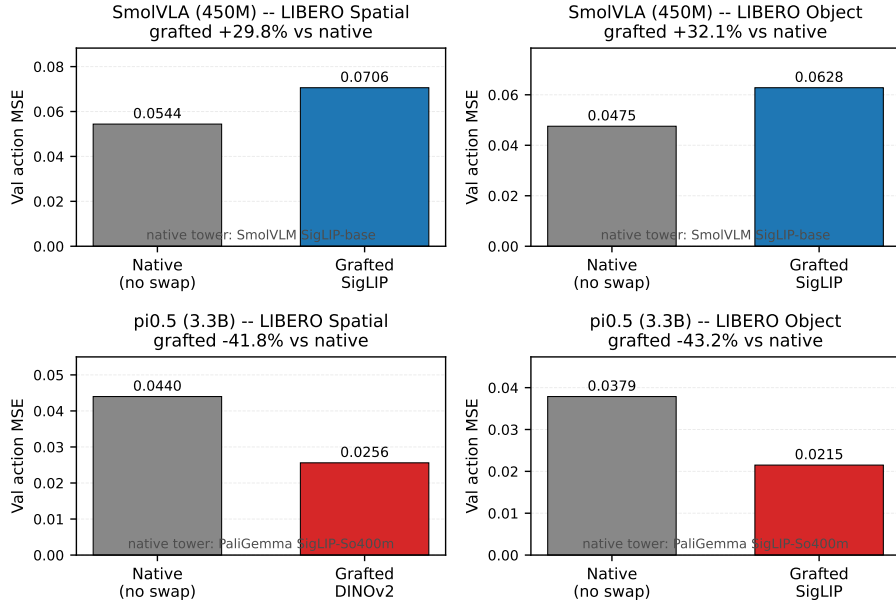


Figure 2: Native-vs-grafted offline MSE differs sharply between the two tested released backbones, all percentages reported as relative MSE vs native. On SmolVLA the best grafted encoder (SigLIP) is 30–32% higher MSE than the native tower; on $\pi_{0.5}$ the best grafted encoder (DINOv2 on spatial, SigLIP on object) is 42–43% lower MSE than the native PaliGamma SigLIP-So400m tower. We do not interpret this as a causal scale effect (see text); SmolVLA and $\pi_{0.5}$ differ in many architectural and pretraining factors besides parameter count.

Backbone	Encoder	Suite	P1 MSE	P2 MSE	Δ
SmolVLA	SigLIP	spatial	0.0682	0.0534	-21.8%
SmolVLA	FastViT	spatial	0.0898	0.0763	-15.0%
$\pi_{0.5}$	SigLIP	spatial	0.0275	0.0238	-13.4%
$\pi_{0.5}$	FastViT	spatial	0.0278	0.0252	-9.1%

Table 6: P2 LoRA ablation on the `libero_spatial` suite, seed 42. P1 MSE is the projector-only baseline taken from the main matrix (seed-42 only); P2 MSE is the same configuration with a rank-8 LoRA adapter unfrozen inside the encoder. Δ is reported as $(P2 - P1)/P1$; negative values mean LoRA improves over P1. This is a gate-level ablation: one seed, one suite, two encoders, two backbones.

gate-level matrix: one seed (42), one suite (`libero_spatial`), two encoders (`{SigLIP, FastViT}`), two backbones (`{SmolVLA, $\pi_{0.5}$ }`), for four P2 cells in total. Results are summarized in Table 6.

Two observations follow. First, the gate-level rank-8 LoRA adapter improves the projector-only baseline in all four tested cells, with the relative MSE reduction ranging from 9% on the $\pi_{0.5}$ ×FastViT cell to 22% on the SmolVLA×SigLIP cell. We read this as qualitative evidence that unlocking encoder capacity does not hurt on the cells we tested; we do not interpret it as a ranking statement, because the gate is a $2 \times 2 \times 1 \times 1$ slice (two encoders, two backbones, one suite, one seed) with no DINOv2 or RepViT under P2. Second, the LoRA gain on SmolVLA recovers most of the native-vs-grafted gap reported in subsection 4.10: the best P2 cell on SmolVLA (SigLIP at 0.0534) is within 2% of the native tower’s spatial MSE of 0.0544, indicating that LoRA on a grafted encoder closes the 30–32% relative-MSE-vs-native gap to near-parity with the native vision tower on SmolVLA.

We also note a more tentative observation. On $\pi_{0.5}$ `libero_spatial` seed 42, the P2 SigLIP cell reaches 0.0238, which is below the P1 DINOv2-small seed-42 cell of 0.0243 on the same backbone-suite-seed slice (this is a single-seed value from the released logs, not the seed-averaged mean of

Encoder	AvgPool	AttnPool	Perceiver	Trainable (M)
SigLIP	0.0626	0.0914	0.0518	0.74 / 1.54 / 59.88
DINOv2	0.0649	0.0986	0.0555	0.37 / 0.80 / 59.52

Table 7: Pooling sensitivity ablation on SmolVLA \times `libero_spatial`, seed 42. Each cell is single-seed validation MSE under three pooling choices that replace the main matrix’s 8×8 adaptive average pool. The last column reports the trainable parameter count of the (projector + pooling) head for each of the three pooling options in the same order (AvgPool / AttnPool / Perceiver). Best-per-row in bold.

Table 1). Taken at face value this would suggest that unlocking encoder capacity reverses the P1 ranking from DINOv2 to SigLIP on $\pi_{0.5}$ – a P1→P2 ranking flip. We refuse to claim it. The current P2 matrix has $N=1$ seed, 1 suite, and only 2 of the 4 encoders (no P2 DINOv2 and no P2 RepViT), so the comparison is between a P2 SigLIP cell and a P1 DINOv2 cell at matched seed but unmatched protocol – which is not a controlled test of the P1→P2 ranking. We therefore tabulate this as a hypothesis for future work rather than a claim, and the gate-level scope is re-emphasized in subsection 5.5. A full P2 sweep over the same $4 \times 2 \times 2$ design as the main matrix is required before any ranking-flip statement can be made.

4.12 Targeted pooling ablation on SmolVLA-spatial-seed42

The main matrix uses a deterministic 8×8 adaptive average pooling stage between the encoder token grid and the linear projector. A natural concern is that the encoder ranking we report is in fact a ranking of how well each encoder’s token grid happens to survive that particular pooling choice. We test this directly by replacing the adaptive-average pool with two alternatives while holding the rest of the grafting pipeline fixed: a single-head cross-attention pool (`attnpool`, 64 queries attending into the encoder tokens) and a small Perceiver-IO resampler (`perceiver`, 64 latents, two cross-attention blocks). We sweep the two pooling alternatives across two encoders (SigLIP, DINOv2) on the `libero_spatial` suite under SmolVLA, seed 42, giving six ablation cells in total alongside an `avgpool` baseline re-run under the identical pooling-ablation harness (these `avgpool` numbers are from this self-contained ablation sweep and differ slightly from the main-matrix seed-42 cells, which use the full training pipeline). Results are summarized in Table 7.

Three observations follow. First, the pooling ordering is consistent across both encoders on this slice: `Perceiver` \prec `AvgPool` \prec `AttnPool` on `val_MSE` for SigLIP and for DINOv2 alike, so the choice of pooling does not depend on the encoder. Second, *the SigLIP–DINOv2 ordering is preserved* under all three pooling options on the SmolVLA `libero_spatial` seed-42 slice we test ($0.0626 < 0.0649$ for AvgPool, $0.0914 < 0.0986$ for AttnPool, $0.0518 < 0.0555$ for Perceiver). This targeted ablation rules out pooling choice as an obvious explanation for the SmolVLA SigLIP-over-DINOv2 result on `libero_spatial`-seed42, but does not establish pooling invariance across all backbones, suites, encoder pairs or seeds. Third, the Perceiver-IO resampler does improve absolute `val_MSE` by roughly 17% for SigLIP and 14% for DINOv2 over the AvgPool baseline, but it carries roughly 60M trainable parameters in its cross-attention stack versus 0.74M / 0.37M for the AvgPool projector head — a near $100\times$ trainable-parameter cost for a single-digit absolute MSE reduction. The single-head AttnPool baseline, by contrast, is strictly worse than the deterministic AvgPool on both encoders. We therefore keep AvgPool as the main-matrix protocol on cost–benefit grounds while documenting that a Perceiver-IO head is the right choice if absolute action MSE is the operational objective and the additional 60M trainable parameters are acceptable.

4.13 Sanity controls: zero-image and shuffled-image baselines and native-encoder-through-graft-interface control

The candidate-encoder matrix above compares four foreign encoders inside the same grafting wrapper. Two questions about the wrapper itself are not answered by that matrix. *First*, how much of the offline action-MSE signal is actually carried by the visual stream, as opposed to the language prompt, state prior or action prior that the frozen backbone already provides? *Second*, is the grafting wrapper (AdaptiveAvgPool + LayerNorm + linear projector) neutral with respect to the native vision tower of each released checkpoint, so that the native-vs-grafted comparison in subsection 4.10 is measuring an encoder swap rather than a wrapper-induced shift? *Third*, is the visual signal that the encoder

actually uses the fine-grained spatial-action correspondence in the image, or a low-frequency image statistic such as the pixel histogram? We answer all three with a sanity-control block of 12 additional runs (one zero-image cell, one shuffled-image cell, and one native-encoder-through-graft-interface control cell on each of the four (backbone, suite) pairs at seed 42), trained under the same 2,000-step projector recipe used for the candidate-encoder matrix.

Zero-image baseline. The zero-image baseline replaces the input RGB image with an all-zero tensor of the same 224×224 shape at every train step and every evaluation step, while leaving the rest of the grafted pipeline unchanged: the SigLIP-base encoder still runs forward on the all-zero input, the AdaptiveAvgPool→LayerNorm→linear projector is still trained for 2,000 steps, and validation MSE is computed on the same held-out window set used for the main matrix. Because the encoder receives no visual signal, any non-trivial information about the demonstration action chunk has to come from the language prompt, the proprioceptive state vector and the action prior carried by the frozen backbone. The vision gap of an encoder is then the relative MSE drop from this zero-image baseline to that encoder’s seed-42 candidate cell.

Shuffled-image baseline. The shuffled-image baseline replaces the input RGB image with a per-image pixel-shuffled version: at every train step and every evaluation step, the spatial positions of the pixels within each 224×224 image are permuted uniformly at random, with the permutation tied across the three RGB channels so that each (R,G,B) triple stays attached to its original pixel and only its (x, y) location changes. This destroys all spatial structure that ties the image to the demonstration action while preserving the marginal pixel histogram (and therefore the global mean, variance, and per-channel colour distribution) of every individual image. The encoder’s activation distribution stays much closer to its training manifold than under the zero-image baseline, so the shuffled-image MSE isolates “how much of the visual contribution comes from the spatial-action correspondence that the encoder extracts” from “how much MSE shift is driven purely by an activation-distribution shift off the encoder’s training manifold”. The shuffle-tolerance gap of an encoder is the relative MSE drop from this shuffled-image baseline to that encoder’s seed-42 candidate cell; a small shuffle-tolerance gap means the encoder ranking on that cell is consistent with the encoder using low-frequency image statistics rather than fine-grained spatial structure.

Native-encoder-through-graft-interface control. The native-encoder-through-graft-interface control — a *native-through-interface* control, for short — takes the native vision tower of each backbone — the SmolVLM SigLIP vision tower for SmolVLA and the PaliGemma SigLIP-So400m vision tower for $\pi_{0.5}$, both extracted directly from the loaded policy checkpoint — and routes it through the same AdaptiveAvgPool + LayerNorm + linear projector that all candidate encoders use. The projector is trained for the same 2,000-step budget and the rest of the recipe is matched cell-by-cell to the main matrix. The wrapper gap of a backbone is the relative MSE change from this native-through-interface control cell to the corresponding native-anchor cell in Table 5, which uses the native vision tower with its original `multi_modal_projector` or `connector` path. If the wrapper is neutral, the two cells should match to within seed noise; if the wrapper is non-neutral the sign of the gap reveals whether the wrapper is helping or hurting the native path.

Visual dependence and backbone scale. Removing the visual stream raises offline action MSE by +12.77% on SmolVLA-spatial and +25.28% on SmolVLA-object relative to the seed-42 SigLIP-base cell, and by +50.54% on $\pi_{0.5}$ -spatial and +95.54% on $\pi_{0.5}$ -object. The vision contribution is therefore roughly 13–25% of cell MSE on the small backbone and rises to 50–95% on the large backbone (here $\pi_{0.5}$ -3.3B vs SmolVLA-450M). We deliberately do *not* present this as a scaling law: we have only two backbones and four (backbone, suite) cells under a single grafting interface, and SmolVLA and $\pi_{0.5}$ differ in many factors besides parameter count (subsection 4.10, subsection 5.5). We therefore frame it as a two-backbone observation/hypothesis: visual dependence is substantially larger on the tested large backbone than on the tested small backbone, and a broader sweep of backbones (and a shuffled-image complement to the zero-image control) would be required before any general “vision-utility-scales-with-size” claim could be defended.

Wrapper non-neutrality across backbones. Routing the native vision tower through the grafting wrapper raises MSE by +55.81% on SmolVLA-spatial and +45.45% on SmolVLA-object (wrapper hurts the native path), but reduces MSE by −49.84% on $\pi_{0.5}$ -spatial and −51.94% on $\pi_{0.5}$ -object (wrapper helps the native path). The two backbones therefore disagree on the

Backbone	Suite	zero-image	shuffled-image	SigLIP-base	native-thru-interface	vision-gap	shuffle-gap	wrapper-gap
SmolVLA	spatial	0.07696	0.10133	0.06824	0.08416	+12.77%	+48.49%	+55.81%
SmolVLA	object	0.07638	0.09216	0.06097	0.06950	+25.28%	+51.16%	+45.45%
$\pi_{0.5}$	spatial	0.04135	0.02854	0.02747	0.02153	+50.54%	+3.90%	-49.84%
$\pi_{0.5}$	object	0.04100	0.02562	0.02097	0.01800	+95.54%	+22.18%	-51.94%

Table 8: Sanity controls at seed 42 on each (backbone, suite) pair. `zero-image` is the all-zero RGB baseline; `shuffled-image` is the per-image pixel-shuffle baseline (RGB-channel-tied permutation; pixel histogram preserved, spatial structure destroyed); `SigLIP-base` is the seed-42 candidate-encoder cell from the main matrix at the same backbone, suite and seed; `native-thru-interface` is the native vision tower routed through the fixed grafting protocol (i.e., the native-encoder-through-graft-interface control). `vision-gap` is $(\text{zero-image} - \text{SigLIP-base})/\text{SigLIP-base}$ and measures the relative MSE increase when the visual stream is removed; larger values mean visual signal is more load-bearing. `shuffle-gap` is $(\text{shuffled-image} - \text{SigLIP-base})/\text{SigLIP-base}$ and measures the relative MSE increase when the spatial structure is destroyed but the pixel histogram is preserved; a small shuffle-gap means the encoder is shuffle-tolerant on that cell and the encoder ranking there is consistent with low-frequency image statistics rather than fine-grained spatial-action correspondence. `wrapper-gap` is $(\text{native-thru-interface} - \text{native})/\text{native}$ relative to the matched seed-42 native MSE (every cell in this table is at seed 42, so the wrapper-gap uses the seed-42 native baseline — 0.05401, 0.04779, 0.04292, 0.03746 for SmolVLA-spatial, SmolVLA-object, $\pi_{0.5}$ -spatial, $\pi_{0.5}$ -object respectively — rather than the seed-averaged native MSE in Table 5); positive values mean the wrapper degrades the native tower, negative values mean the wrapper improves the native tower. The vision-gap grows from 12.77–25.28% on SmolVLA to 50.54–95.54% on $\pi_{0.5}$ (13–25% vs 50–95% in summary). The shuffle-gap is +48–51% on SmolVLA (both suites), +22% on $\pi_{0.5}$ -object, and only +3.9% on $\pi_{0.5}$ -spatial — the latter cell is therefore inside its own within-encoder gap band and we flag it as shuffle-tolerant. The wrapper-gap flips sign across backbones: +45.45% to +55.81% (wrapper hurts) on SmolVLA versus -49.84% to -51.94% (wrapper helps) on $\pi_{0.5}$.

sign of the wrapper effect. A coherent reading is that the SmolVLM SigLIP vision tower already emits a $(B, 64, 960)$ token grid that matches the SmolVLA expert shape, so feeding it through an additional 8×8 AdaptiveAvgPool and a fresh linear projector strictly removes information; on $\pi_{0.5}$, the PaliGemma SigLIP-So400m tower emits a higher-dimensional $(B, 256, 2048)$ grid and the wrapper’s 16×16 pool and linear projector appear to provide a useful bottleneck or regularisation rather than a destructive compression. The wrapper non-neutrality has two immediate implications for the rest of the paper. *First*, the 42–43% best-grafted-minus-native MSE gap on $\pi_{0.5}$ reported in Table 5 cannot be interpreted as encoder superiority: the native-encoder-through-graft-interface control alone explains -50% of the native MSE on $\pi_{0.5}$, showing that the native-vs-grafted gap is wrapper-induced (interface-induced) rather than candidate-encoder-substitution induced. *Second*, the SigLIP-vs-DINOv2 within-interface comparison remains the cleanest contrast in the paper because both encoders cross the same fixed grafting protocol; we now read the SigLIP-vs-DINOv2 ranking as an encoder-quality contrast inside a fixed (and demonstrably non-neutral) grafting interface rather than as an encoder-quality contrast against the native path. We emphasise that the fixed-grafting-protocol qualifier travels with every encoder-comparison claim in this paper.

Encoder gap vs. the vision-contribution band. The SigLIP-vs-DINOv2 mean-MSE gap in the candidate matrix is roughly 1.7% on $\pi_{0.5}$ -object, 4.1% on $\pi_{0.5}$ -spatial, 7.0% on SmolVLA-object, and 4.0% on SmolVLA-spatial, all under the seed-averaged reading from Table 1; the largest SigLIP-vs-DINOv2 cell-level gap reaches roughly 12% on the most contested suite. All four cell-level gaps sit inside the vision-contribution band reported above (13–25% on SmolVLA, 50–95% on $\pi_{0.5}$), which is *consistent with — though not by itself proof of —* the candidate-encoder ranking reflecting real sample-level visual-signal differences rather than a prior-dominated artifact. The gap is also compatible with several alternative explanations that the zero-image control alone cannot rule out: differences in input preprocessing across encoders, activation-distribution shifts that bias the projector training, projectability into the backbone hidden space, or interface-matching effects between a given encoder output shape and the wrapper’s fixed pool/projector head. Sorting these apart requires further sanity controls, which we list below.

Shuffled-image vs. zero-image. The zero-image baseline is a strong but out-of-distribution (OOD) ablation: zeroing the RGB input shifts the encoder’s activation statistics off its training manifold and

therefore conflates two distinct questions — “how much does the visual signal contribute?” and “how much MSE shift is driven purely by an activation-distribution shift?”. The shuffled-image baseline preserves the encoder’s marginal activation distribution (the pixel histogram is unchanged) while destroying the spatial structure that ties the image to the demonstration action, and therefore separates these two questions. The two baselines also implement two qualitatively different policy regimes. Under *zero-image* the vision tower sees a constant all-zero input and its output is approximately a constant bias, so the projector head can learn to ignore the visual stream entirely and recover whatever the language prompt, state and action priors provide. Under *shuffled-image* the vision tower sees dynamically varying but spatially meaningless input, its output is non-constant but *misleading*, and the policy is forced to integrate an incorrect visual signal rather than ignore it. We therefore expect the shuffled-image MSE to be *above* the zero-image MSE on cells where the encoder is genuinely using fine-grained spatial structure, and to be *close to or below* the zero-image MSE on cells where the encoder is mostly using low-frequency image statistics (because zero-image is then the heavier OOD shift).

The pattern we observe (Table 8) is backbone-and-suite-dependent and falls into three regimes. (i) On SmolVLA-*spatial* and SmolVLA-*object* shuffled-image MSE (0.10133, 0.09216) is substantially above zero-image MSE (0.07696, 0.07638), so the shuffle-gap (+48.49%, +51.16%) is more than double the vision-gap (+12.77%, +25.28%). The SmolVLA encoder is therefore using real spatial-action correspondence on both suites, not the pixel histogram — forcing the policy to integrate a histogram-matched but spatially scrambled image is strictly worse than letting it ignore the visual stream. (ii) On $\pi_{0.5}$ -*object* the shuffle-gap is +22.18% while the vision-gap is +95.54%, so destroying spatial structure costs roughly a quarter of the full visual-contribution budget. The SigLIP-vs-DINOv2 within-wrapper cell-level encoder gap on this suite (1.7–7%) sits well below the 22% shuffle-gap, so we read the $\pi_{0.5}$ -*object* encoder ranking as still validated by a genuine vision-utility band: encoder differences on this suite are inside the shuffle-tolerance band, but they are not within the *shuffle-gap* band itself. (iii) On $\pi_{0.5}$ -*spatial* the shuffle-gap is only +3.90% while the vision-gap is +50.54%, so $\pi_{0.5}$ on *libero_spatial* loses almost nothing when the spatial structure is destroyed as long as the pixel histogram is preserved. We make this limitation explicit: the SigLIP-vs-DINOv2 cell-level gap on $\pi_{0.5}$ -*libero_spatial* (1.7–12% MSE between SigLIP and DINOv2 within the wrapper, depending on the cell) is *comparable to* the 3.9% shuffle-tolerance band on the same suite — for several cells it is even smaller — so the within-wrapper SigLIP-vs-DINOv2 ranking on this specific suite may reflect low-frequency image statistics (colour distribution, texture marginals) rather than fine-grained spatial-action correspondence. We therefore treat $\pi_{0.5}$ -*libero_spatial* as the weakest of the supporting cells in our main claim and limit the claim about it accordingly in subsection 5.5. The remaining three (backbone, suite) cells (SmolVLA-*spatial*, SmolVLA-*object*, $\pi_{0.5}$ -*object*) are validated by both the zero-image and shuffled-image controls.

Vision usage is backbone-and-suite-dependent. Combining the zero-image and shuffled-image controls gives us a sharper picture than either control alone: the way the grafted encoder uses the visual input is not a single mechanism that transfers across backbones and suites. SmolVLA on both suites uses genuine spatial-action correspondence (large vision-gap, even larger shuffle-gap). $\pi_{0.5}$ on *libero_object* also uses real spatial structure, but the shuffle-tolerance band (+22%) is narrower than on SmolVLA and the encoder ranking is correspondingly less robust to noise. $\pi_{0.5}$ on *libero_spatial* sits in a low-frequency-statistic-dominated regime where the encoder ranking is shuffle-tolerant and where within-wrapper encoder-comparison claims should be interpreted as weaker than the SmolVLA cells. We treat this backbone-and-suite dependence of vision usage as an unexpected secondary contribution of this paper: vision-utility is not a property of the backbone or of the suite in isolation but of the (backbone, suite) cell, and a single shuffled-image control surfaces this dependence at low cost. Within this caveat, the present zero-image-plus-shuffled-image finding still rules out the degenerate case of “vision is not used at all” on three of the four (backbone, suite) cells under the fixed grafting protocol, which is the load-bearing claim we make in this paper.

4.14 Training-loss plateau evidence for the 2,000-step budget

A standing question for any fixed-budget projector recipe is whether the budget is the binding constraint on the encoder ranking. The per-encoder training-loss curves for each (backbone, suite) pair in Figure 3 confirm that all evaluated encoders reach a plateau region by step 1,500–2,000 on both backbones; the 2,000-step budget is not bottlenecking encoder ranking.

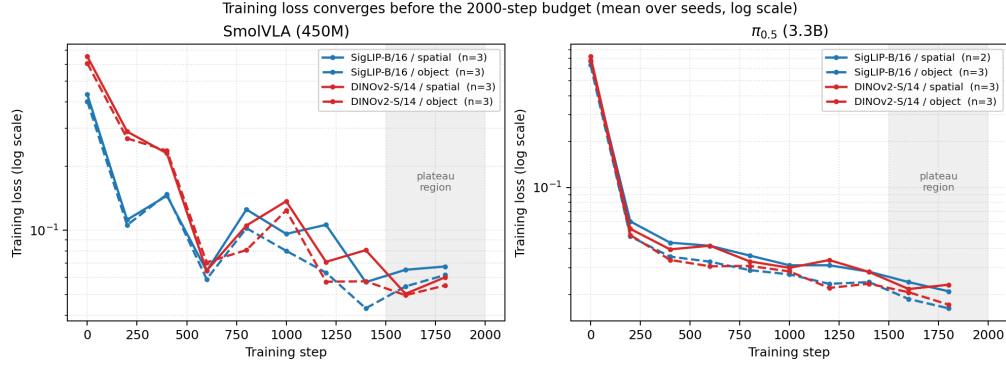
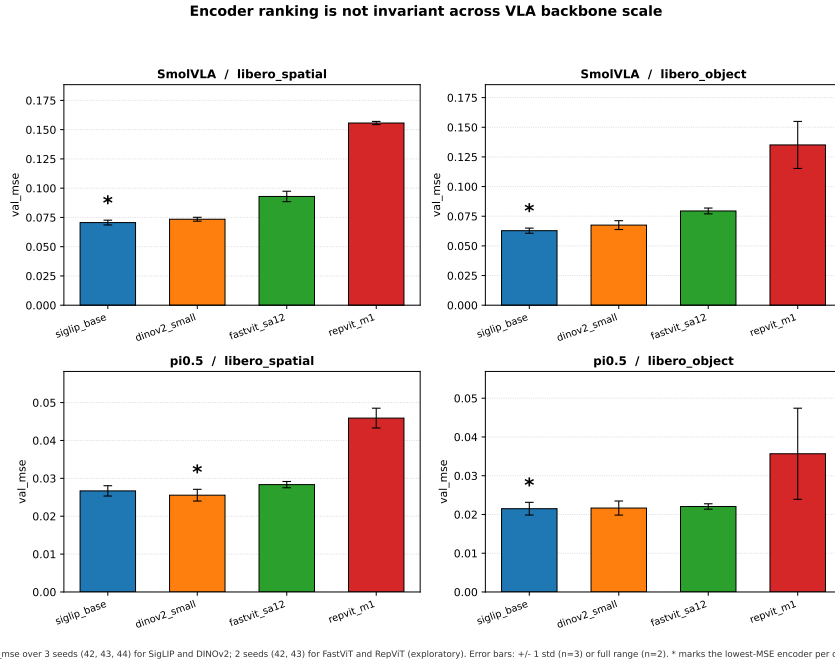


Figure 3: Training-loss curves for the four candidate encoders on SmolVLA and $\pi_{0.5}$ on the two LIBERO suites, seed 42. All evaluated encoders reach a plateau region by step 1,500–2,000 on both backbones, supporting our wording in subsection 3.3 that conclusions are reported under a fixed 2,000-step projector budget rather than as “best encoder absolutely”.



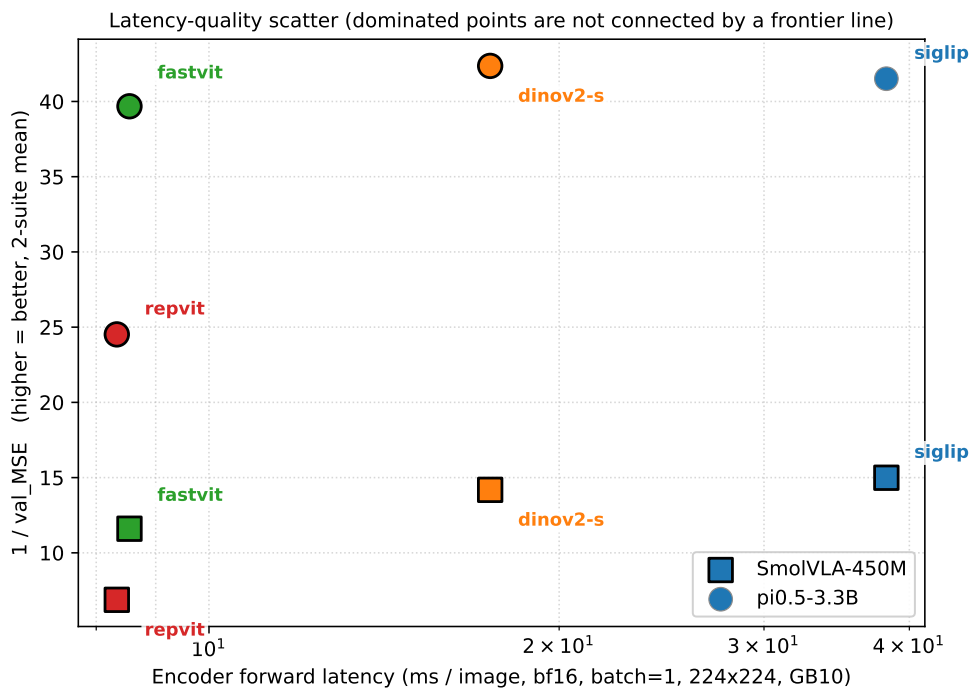
Bars: mean val_mse over 3 seeds (42, 43, 44) for SigLIP and DINOv2; 2 seeds (42, 43) for FastViT and RepViT (exploratory). Error bars: +/- 1 std (n=3) or full range (n=2). * marks the lowest-MSE encoder per cell. Lower is better.

Figure 4: Per-cell offline action MSE on `libero_spatial` and `libero_object` under the frozen-backbone grafting protocol (the same data as Table 1). SigLIP is the lowest-mean-MSE encoder on both suites for SmolVLA-450M; DINOv2-small is the lowest-mean-MSE encoder on the $\pi_{0.5}$ -spatial suite; on $\pi_{0.5}$ -object the three strongest encoders sit in a near-tie band where the seed-44 top-1 identity reverses to SigLIP relative to the seed {42, 43} reading. SigLIP and DINOv2 are at three seeds per cell (seeds {42, 43, 44}); FastViT and RepViT are at two seeds per cell (seeds {42, 43}). Note different y -axis ranges across backbones.

5 Discussion

5.1 Main takeaway

Our central observation is descriptive and task-dependent: under a controlled frozen-backbone grafting protocol, the small-backbone encoder winner does not reliably select the large-backbone top tier. SigLIP is the lowest-mean-MSE encoder on SmolVLA across both LIBERO suites (with 3/3 seeds in the SigLIP-vs-DINOv2 direction on each suite). On $\pi_{0.5}$ -libero_spatial DINOv2-small



Note: latency measured with GB10 co-occupied by another task; ranking valid, absolutes inflated.

Figure 5: Latency–quality scatter for the four encoders on SmolVLA-450M (squares) and $\pi_{0.5}$ -3.3B (circles), averaged over the two LIBERO suites and over the seeds available per cell (three for SigLIP/DINOv2, two for FastViT/RepViT). Dominated points are not connected by a frontier line; this figure is descriptive of the within-backbone tradeoff and should not be read as evidence that $\pi_{0.5}$ is “higher quality” than SmolVLA in absolute terms, since action normalization, token count and sampling differ across the two backbones.

is the lowest-mean-MSE encoder (with 3/3 seeds in the DINOv2-vs-SigLIP direction, although the seed-44 cell is a numerical near-tie at $\Delta = 0.00001$ MSE so the within-seed margin at that seed should not be over-read). On $\pi_{0.5}$ -libero_object the three strongest encoders (SigLIP 0.02149, DINOv2 0.02166, FastViT 0.02206) sit in a near-tie band within 2.7% relative of each other, and the seed-level top-1 identity is not stable to a single additional seed (SigLIP<DINOv2 at seed 44, DINOv2<SigLIP at seeds 42 and 43). The suite-level summary is that 3/4 backbone-suite SigLIP-vs-DINOv2 directions support the backbone-dependent top-tier pattern, with $\pi_{0.5}$ -libero_object as the lone exception; we treat this 3/4 as the load-bearing inferential summary, with the 11/12 seed-level cell split as descriptive support. At the (backbone, suite) level, the sanity controls (subsection 4.13, Table 8) validate three of the four cells under both the zero-image and shuffled-image controls; the fourth, $\pi_{0.5}$ -libero_spatial, is shuffle-tolerant (shuffle-gap +3.9%, comparable to the 1.7–12% within-wrapper SigLIP-vs-DINOv2 cell-level gap on the same suite), and we treat it as the weakest supporting cell, with the implication discussed in subsection 5.5 below. The finer 11/12 vs 1/12 cell-level split is descriptive evidence consistent with the same pattern (Table 2); we do not defend it as independent inferential evidence because the cells share seeds, projector initialization, and validation episode order, and so they are not pseudo-independent samples. We deliberately do *not* call this a full ranking inversion: the cross-backbone Spearman correlation stays positive on both suites (+0.80, +1.00) because the worst encoder in the pool is reliably the worst encoder on both backbones. The claim we are willing to defend is narrower: the top-1 encoder selected on SmolVLA does not reliably select the top-1 encoder on $\pi_{0.5}$ under this offline diagnostic, and the partial bottom-of-pool ordering transfers while the top-1 choice does not. The $\pi_{0.5}$ -libero_spatial seed-44 near-tie supports rather than weakens this claim, since it shows the large-backbone top tier is a narrow-margin competition unsuited for small-backbone top-1 commitment. At a minimum this argues that future encoder-comparison papers should report at least two backbones at different scales *and* a robustness check at a third seed before stating “encoder X is best for VLA” as an architectural prescription, and that a small grafting

sweep on the target released backbone is a cheap way to confirm or refute the small-VLA top-1 choice before any expensive downstream training.

A second observation emerges from the native-vs-grafted comparison in subsection 4.10 (Table 5, Figure 2) once the sanity controls in subsection 4.13 are folded in. On the two released backbones we test, the sign of the native-vs-grafted offline MSE comparison differs: on SmolVLA the best grafted encoder is 30–32% higher MSE than the native tower, while on $\pi_{0.5}$ the best grafted encoder is 42–43% lower MSE than the native PaliGemma SigLIP-So400m tower. The new sanity controls reveal that the $\pi_{0.5}$ 42–43% lower-MSE-than-native number is *wrapper-induced (interface-induced) rather than candidate-encoder-substitution induced*, and therefore cannot be read as encoder superiority: the native-encoder-through-graft-interface control (Table 8) shows that routing the native $\pi_{0.5}$ vision tower through the fixed grafting protocol *alone*, with no candidate encoder substitution, already moves MSE from native by -49.84% on `spatial` and -51.94% on `object` — essentially recovering the 42–43% best-grafted gap without ever substituting an encoder. We therefore reinterpret the $\pi_{0.5}$ native-vs-grafted gap as “the wrapper itself is a non-neutral path that happens to help the $\pi_{0.5}$ native tower”, not as “a candidate encoder is intrinsically better than the native tower”. Symmetrically, the wrapper degrades the SmolVLA native path by $+45\text{--}56\%$, which contributes to the 30–32% best-grafted-vs-native gap on SmolVLA in the opposite direction. The wrapper effect therefore has opposite sign across the two backbones, and the candidate-encoder comparison that survives this reinterpretation cleanly is the within-wrapper SigLIP-vs-DINOv2 contrast, because both encoders cross the same wrapper. We are deliberately careful not to interpret the cross-backbone sign of the wrapper effect as a causal scale effect either: SmolVLA and $\pi_{0.5}$ differ in many architectural and pretraining factors besides parameter count, so the most we can say descriptively is that the wrapper effect flips sign between the two released checkpoints, and that the sign on either checkpoint should not be assumed to transfer to a third released backbone without re-measurement. The targeted pooling ablation in subsection 4.12 further shows that the SigLIP-DINOv2 ordering is preserved across three pooling choices on SmolVLA-`libero_spatial-seed42`, which rules out token-pooling as an obvious explanation for the SmolVLA SigLIP-over-DINOv2 result on that slice but does not establish pooling invariance across all backbones, suites, encoders or seeds.

5.2 Seed-44 sensitivity and the noise-dominated suite

The seed-44 robustness check exposes a regime distinction between the two LIBERO suites that we did not anticipate from the seed {42, 43} data alone, and that we think future encoder-comparison papers should adopt as a routine sanity check. On $\pi_{0.5}$ -`libero_spatial` the cross-encoder DINOv2-vs-SigLIP gap is up to 13% relative on the strongest seed in the {42, 43, 44} set and the direction is preserved across all three seeds; we read this as a regime where the cross-encoder signal exceeds seed noise. On $\pi_{0.5}$ -`libero_object` the three strongest encoders are within 2.7% relative of each other under the three-seed mean (0.02149 vs 0.02166 vs 0.02206), the seed-level top-1 identity flips between SigLIP and DINOv2 across the three seeds, and a third seed at the SigLIP/DINOv2 cells alone is enough to reverse the rank-order claim that the seed-{42, 43} data alone would have supported. This is itself part of our finding: the cross-backbone top-1 question is meaningful only on suites where the cross-encoder gap exceeds seed noise (`libero_spatial`: gap up to 13%, stable; $\pi_{0.5}$ -`libero_object`: gap $< 3\%$ at the top of the pool, unstable). For the noise-dominated suite the operationally honest statement is that the top three encoders are within seed-level noise of each other, and the appropriate selector is one of (a) running additional seeds until the gap exceeds noise or (b) tabulating the near-tie band explicitly and selecting on a secondary axis (latency, parameter count, deployment constraints) rather than on offline MSE alone.

5.3 Vision usage is backbone-and-suite-dependent

A secondary observation that emerges only once the zero-image and shuffled-image controls of subsection 4.13 are both available is that the grafted encoder does not use the visual input in a single uniform way across our four (backbone, suite) cells. The four cells fall into three regimes, which we treat as an unexpected contribution of this paper rather than as a clean-up footnote on the main matrix.

Real spatial-action correspondence (SmolVLA, both suites). On SmolVLA the vision-gap is $+12.77\text{--}25.28\%$ and the shuffle-gap is $+48.49\text{--}51.16\%$ — substantially *larger* than the vision-gap. The encoder uses spatial structure that the shuffled-image baseline destroys, and a histogram-matched but

spatially scrambled image is strictly worse than no image at all because the projector head is forced to integrate a misleading visual signal rather than learn to ignore it. The SmolVLA encoder ranking on both suites is therefore validated as spatial-correspondence-driven.

Real spatial-action correspondence with a narrower band ($\pi_{0.5}$ -object). On $\pi_{0.5}$ -object the vision-gap is +95.54% and the shuffle-gap is +22.18%, so destroying spatial structure costs roughly a quarter of the visual-contribution budget. The within-wrapper SigLIP-vs-DINOv2 cell-level encoder gap on this suite (1.7–7%) is below the 22% shuffle-tolerance band, so we read the $\pi_{0.5}$ -object encoder ranking as genuinely validated by a real-vision-utility band even if the band is narrower than on SmolVLA.

Low-frequency image statistics dominated ($\pi_{0.5}$ -spatial). On $\pi_{0.5}$ -spatial the vision-gap is +50.54% but the shuffle-gap is only +3.90%. The encoder loses almost nothing when the spatial structure is destroyed as long as the pixel histogram is preserved, which is direct evidence that the encoder is using low-frequency image statistics (colour distribution, texture marginals) rather than fine-grained spatial-action correspondence on this specific suite. The within-wrapper SigLIP-vs-DINOv2 cell-level gap on this suite (1.7–12%) is *larger* than the shuffle-tolerance band, so the SigLIP-vs-DINOv2 ranking on this cell may reflect which encoder happens to emit a more useful low-frequency activation distribution rather than which encoder reads spatial structure better. We flag this in subsection 5.5 below.

The operational reading is that vision-utility is a property of the (backbone, suite) cell rather than of the backbone alone or the suite alone. A successor study evaluating encoders on a single (backbone, suite) cell could therefore draw qualitatively different conclusions depending on which cell it picks, and the shuffled-image control turns out to be a cheap but high-information test that surfaces this dependence at the cost of a single additional projector run per cell. We recommend that future encoder-comparison studies run both the zero-image and shuffled-image controls as a routine pair.

5.4 Hypotheses for the wrapper non-neutrality and the cross-backbone sign difference

The native-encoder-through-graft-interface control of subsection 4.13 shows that the cross-backbone sign of the native-vs-grafted MSE difference is substantially attributable to the fixed grafting protocol itself being non-neutral with opposite sign across the two backbones (wrapper-gap +45.45% to +55.81% on SmolVLA, -49.84% to -51.94% on $\pi_{0.5}$). We do not have a mechanistic explanation for this opposite-sign wrapper effect, but we offer two hypotheses that are consistent with the sanity-control data and testable in future work. First, the SmolVLM SigLIP vision tower already emits a (B , 64, 960) token grid matched to the SmolVLA expert, so feeding it through an additional 8×8 AdaptiveAvgPool and a fresh linear projector strictly removes information — there is no compression bottleneck for the wrapper to add value at on this backbone. By contrast, the PaliGemma SigLIP-So400m tower on $\pi_{0.5}$ emits a higher-dimensional (B , 256, 2048) grid, and the wrapper’s 16×16 pool and linear projector appear to provide a useful bottleneck or regularisation rather than a destructive compression. Second, on $\pi_{0.5}$ the Gemma expert attends across 256 tokens and may be more sample-efficient at re-interpreting an unfamiliar token stream than the SmolVLM expert is at 64 tokens, so the marginal cost of crossing an extra projector may shrink (and even flip to a benefit) once the expert is large enough to compensate. Both hypotheses predict that the wrapper-gap should shrink as the projector capacity grows and as the expert hidden size grows, and we leave the quantitative tests to future work.

5.5 Limitations

This study has several limitations that we wish to be explicit about rather than hide.

Preprocessing-protocol confound. All grafted runs in this paper share a unified 224×224 preprocessing path (bilinear resize, the unified normalization inherited from the backbone’s vision-input pipeline) so that every encoder is exposed to the same input distribution. This unified path may understate encoders whose pretrained normalization or native input resolution differs from the unified protocol — in particular, DINOv2 is natively trained at 518×518 with ImageNet normalization, whereas SigLIP base/16 is natively at 224×224 with $\mu=\sigma=0.5$ normalization. Preprocessing sensitivity is a known threat to validity that we do not quantify here; the present ranking should be

read as conditional on the unified preprocessing path described in subsection 3.2, and a per-encoder official-preprocessing comparison is a natural follow-up.

No closed-loop success claim under embodiment mismatch. We do not report closed-loop success because native released checkpoints collapse under embodiment mismatch; therefore this paper makes no deployment or success-rate claim. The action-MSE numbers in this paper are an offline diagnostic and should not be used as evidence of policy deployment readiness.

Shuffle-tolerance of the $\pi_{0.5}$ -spatial ranking. We note that the within-wrapper SigLIP-vs-DINOv2 encoder ranking on $\pi_{0.5}$ -libero_spatial should be interpreted cautiously: the shuffled-image MSE on this cell is only 3.9% worse than the real-image MSE, comparable to or smaller than the 1.7–12% within-wrapper SigLIP-vs-DINOv2 cell-level gap on the same suite. This means the SigLIP-vs-DINOv2 ranking on $\pi_{0.5}$ -libero_spatial may reflect low-frequency image statistics rather than fine-grained spatial-action correspondence, and we treat this cell as the weakest supporting cell in our main claim. The other three cells (SmolVLA-spatial, SmolVLA-object, $\pi_{0.5}$ -object) remain validated by both the zero-image *and* shuffled-image controls of subsection 4.13: the $\pi_{0.5}$ -object vision usage is validated by the larger 22% shuffle-tolerance band on that cell. The shuffled-image control is precisely the test that surfaces this fragility on $\pi_{0.5}$ -spatial.

Two-to-three seeds per cell. Each (backbone, suite, encoder) cell has $N \in \{2, 3\}$ seeds: SigLIP and DINOv2 are at $n=3$ (seeds 42, 43, 44), and FastViT and RepViT are at $n=2$ (seeds 42, 43, with seed 44 deferred to future work). With few seeds, standardized effect sizes are unstable and paired t -tests have low power; we therefore report directional consistency as our load-bearing statistic and treat Cohen’s d and paired t -values as descriptive only. On $\pi_{0.5}$ -libero_object the top three encoders (SigLIP 0.02149, DINOv2 0.02166, FastViT 0.02206) form a near-tie band where the seed-level top-1 identity flips across the three seeds; a fourth seed on the SigLIP-vs-DINOv2 pair on $\pi_{0.5}$ -object is an important follow-up.

Offline action MSE rather than closed-loop success. We report validation action MSE on a held-out episode split rather than closed-loop success rates. The reason is that the released SmolVLA and $\pi_{0.5}$ checkpoints were trained on SO-100 trajectories with a six-degree-of-freedom action schema, while LIBERO uses a seven-degree-of-freedom Franka schema; zero-shot closed-loop success is therefore near zero for both native and grafted variants and would provide essentially no signal. Offline action MSE is the right proxy under this mismatch — it measures whether the grafted encoder lets the backbone reproduce the demonstration policy — but it is not a substitute for embodied success, and offline MSE does not necessarily correlate with closed-loop rollout success because of compounding error, state-distribution shift and multi-modal action ambiguity. We therefore frame every conclusion in this paper as an *offline diagnostic* under embodiment mismatch and do not claim closed-loop deployment improvement.

Two released backbones at different scales, not isolated scale. We test two released VLA backbones (SmolVLA-450M and $\pi_{0.5}$ -3.3B) that differ in many factors besides parameter count: language backbone, action expert, hidden size, token count, native vision tower, pretraining data, projector architecture and native image preprocessing. We therefore describe the native-vs-grafted sign difference as occurring *across the two released backbones we test*, not as caused by backbone scale; the comparison is scale-correlated but architecture-confounded.

Projector bottleneck risk. The grafted policy has only a single linear projector (0.37–1.58M parameters depending on encoder output dimension and target backbone hidden size). One might worry that the ranking we observe is really a ranking of which encoder happens to be most “linear-projectable” into the backbone’s hidden space, rather than a ranking of encoder quality. The gate-level LoRA ablation in subsection 4.11 improves all four tested cells, which is qualitative evidence against a projector capacity ceiling driving the ranking, but the ablation has only one seed, one suite, and two of four encoders, so it does not control the cross-encoder ranking under P2.

Frozen-LM path dependence. Our main matrix freezes the language model and the action expert. This is required for a fair encoder comparison but it means our top-1 observation is strictly under *zero gradient flow into the backbone*. A LoRA fine-tune of the expert might allow a weaker encoder to “catch up” or it might further amplify the gap; we cannot tell from the current data.

Wrapper non-neutrality as a methodological contribution. The native-encoder-through-graft-interface control of subsection 4.13 demonstrates that the fixed grafting protocol itself shifts native MSE by +45–56% on SmolVLA and by –50–52% on $\pi_{0.5}$ at seed 42, with opposite sign across the two backbones. The within-interface SigLIP-vs-DINOv2 ranking in subsection 4.6 therefore remains the cleanest experimental contrast in this paper because both encoders cross the same fixed grafting protocol, but the native-vs-grafted comparison in subsection 4.10 can no longer be read as “a candidate encoder is intrinsically better than the native vision tower” on $\pi_{0.5}$ — a substantial portion of the 42–43% best-grafted-minus-native gap is explained by the interface alone before any candidate encoder substitution. We retain the native-vs-grafted table as a descriptive contrast and rely on the native-through-interface and zero-image controls for the load-bearing sanity-control statements. The wrapper non-neutrality is itself a methodological contribution: benchmarks that swap visual encoders without controlling for the swap interface conflate encoder choice with interface-backbone compatibility, and reporting the fixed-grafting-protocol caveat (plus the native-through-interface control number) is now part of the diagnostic protocol we recommend for any successor encoder-comparison study on released VLA backbones.

P2 LoRA matrix is gate-level. The P2 ablation reported in subsection 4.11 is deliberately gate-level: one seed, one suite (`libero_spatial`), two of the four encoders, two backbones (2 encoders \times 2 backbones = 4 cells in total, no P2 DINOv2 and no P2 RepViT). The seed-42 P2 SigLIP cell on $\pi_{0.5}$ comes in below the seed-matched P1 DINOv2-small cell, which is suggestive of a P1→P2 ordering shift, but the comparison crosses two protocols at a single seed and is not a controlled cross-encoder ranking test under P2. A controlled statement requires a full P2 sweep that matches the main matrix design (4 encoders \times 2 suites \times ≥ 2 seeds per backbone), which we leave to future work.

5.6 Future work

Three directions are most pressing. First, extending the seed-44 robustness check to the FastViT and RepViT cells; combined with the existing seed-44 SigLIP/DINOv2 data this would give a fully uniform $n=3$ matrix across the 4 encoders and upgrade those two cells from exploratory to confirmatory. Second, a follow-up on the shuffle-tolerant `$\pi_{0.5}$ -libero_spatial` cell identified by the shuffled-image control of subsection 4.13 with a finer-grained baseline sweep (per-channel histogram-only, low-pass-only, and patch-level shuffle variants) to pin down which low-frequency statistic is driving the encoder ranking on that suite. Third, once an embodiment-matched dataset is available, a true closed-loop evaluation with the same fixed grafting protocol to test whether the offline top-1 observation translates to closed-loop success in the same direction; this is the only experiment that can upgrade the current claim from an offline diagnostic to a deployment-relevant prescription.

References

- [1] J. L. Ba, J. R. Kiros, and G. E. Hinton. Layer normalization. *arXiv preprint arXiv:1607.06450*, 2016.
- [2] L. Beyer, A. Steiner, A. S. Pinto, A. Kolesnikov, X. Wang, D. Salz, M. Neumann, I. Alabdulmohsin, M. Tschannen, E. Bugliarello, et al. PaliGemma: A versatile 3B VLM for transfer. *arXiv preprint arXiv:2407.07726*, 2024.
- [3] J. Bjorck, F. Castaneda, N. Cherniadev, X. Da, R. Ding, L. Fan, Y. Fang, D. Fox, F. Hu, S. Huang, et al. VLA-0: Building state-of-the-art VLAs with zero modification. *arXiv preprint arXiv:2510.13054*, 2025.
- [4] P. Intelligence, K. Black, N. Brown, D. Driess, A. Esmail, M. Equi, C. Finn, N. Fusai, M. Y. Galliker, D. Ghosh, et al. $\pi_{0.5}$: a vision-language-action model with open-world generalization. *arXiv preprint arXiv:2504.16054*, 2025.
- [5] M. J. Kim, C. Finn, and P. Liang. Fine-tuning vision-language-action models: Optimizing speed and success. *arXiv preprint arXiv:2502.19645*, 2025.
- [6] M. J. Kim, K. Pertsch, S. Karamcheti, T. Xiao, A. Balakrishna, S. Nair, R. Rafailov, E. Foster, G. Lam, P. Sanketi, et al. OpenVLA: An open-source vision-language-action model. *arXiv preprint arXiv:2406.09246*, 2024.
- [7] S. Li, S. Zhao, J. Wu, Y. Lyu, B. Liu, and Y. Zhu. LIBERO-pro: Benchmarking generalization for vision-language-action models. *arXiv preprint arXiv:2509.21788*, 2025.
- [8] B. Liu, Y. Zhu, C. Gao, Y. Feng, Q. Liu, Y. Zhu, and P. Stone. LIBERO: Benchmarking knowledge transfer for lifelong robot learning. *Advances in Neural Information Processing Systems*, 2023.
- [9] I. Loshchilov and F. Hutter. Decoupled weight decay regularization. *arXiv preprint arXiv:1711.05101*, 2017.
- [10] A. Marafioti, O. Zohar, M. Farré, M. Noyan, E. Bakouch, P. Cuenca, C. Zakka, L. B. Allal, A. Lozhkov, N. Tazi, et al. SmolVLM: Redefining small and efficient multimodal models. *arXiv preprint arXiv:2504.05299*, 2025.
- [11] M. Oquab, T. Darcet, T. Moutakanni, H. Vo, M. Szafraniec, V. Khalidov, P. Fernandez, D. Haziza, F. Massa, A. El-Nouby, et al. DINOv2: Learning robust visual features without supervision. *arXiv preprint arXiv:2304.07193*, 2023.
- [12] J. Shang, K. Schmeckpeper, B. B. May, M. V. Minniti, T. Kelestemur, D. Watkins, and L. Herlant. Theia: Distilling diverse vision foundation models for robot learning. *arXiv preprint arXiv:2407.20179*, 2024.

- [13] M. Shukor, D. Aubakirova, F. Capuano, P. Kooijmans, S. Palma, A. Zouitine, M. Aractingi, C. Pascal, M. Russi, A. Marafioti, et al. SmolVLA: A vision-language-action model for affordable and efficient robotics. *arXiv preprint arXiv:2506.01844*, 2025.
- [14] P. K. A. Vasu, J. Gabriel, J. Zhu, O. Tuzel, and A. Ranjan. FastViT: A fast hybrid vision transformer using structural reparameterization. *arXiv preprint arXiv:2303.14189*, 2023.
- [15] A. Wang, H. Chen, Z. Lin, J. Han, and G. Ding. RepViT: Revisiting mobile CNN from ViT perspective. *arXiv preprint arXiv:2307.09283*, 2023.
- [16] T.-H. Wang, A. Maalouf, G. Rosman, S. Karaman, and D. Rus. On the choice of vision-language backbone for robot policy learning. *arXiv preprint arXiv:2405.05956*, 2024.
- [17] S. Wu, S. Liu, Y. Lyu, S. Liu, Y. Wu, J. Sun, C. Cui, P. P. Liang, Y.-H. Wu, and J. Zhou. LIBERO-plus: In-depth robustness analysis of vision-language-action models. *arXiv preprint arXiv:2511.17850*, 2025.
- [18] X. Zhai, B. Mustafa, A. Kolesnikov, and L. Beyer. Sigmoid loss for language image pre-training. *arXiv preprint arXiv:2303.15343*, 2023.